Wideband Radio Channel Emulation Using Band-stitching Schemes

Ji, Yilin; Fan, Wei; Pedersen, Gert Frølund

Published in:
2020 14th European Conference on Antennas and Propagation (EuCAP)

DOI (link to publication from Publisher):
10.23919/EuCAP48036.2020.9135788

Publication date:
2020

Document Version
Accepted author manuscript, peer reviewed version

Wideband Radio Channel Emulation Using Band-stitching Schemes

Yilin Ji*, Wei Fan*, Gert F. Pedersen*,
*(Affiliation): APMS section, Aalborg University, Aalborg, Denmark, e-mail: yilin@es.aau.dk

***Abstract*—In the fifth-generation (5G) new radio specifications, large signal bandwidth e.g. 400 MHz for frequency range 2 (FR2), is expected to be utilized. Therefore, there is a need to develop channel emulators that can support such large bandwidth. In this paper, we revisit the band-stitching scheme, i.e. combining multiple logic channels of small bandwidth to form a larger total bandwidth. We put a focus on the calibration stage of this scheme, and the effect of the phase jump at the junctions of adjacent subbands on the stitching performance is investigated through simulation.**

***Index Terms*—Channel emulation, band stitching, testing, wideband.**

I. Introduction

Channel emulation techniques have been used extensively for device testing in the industry [1]–[4]. Most of those techniques deploy channel emulators (CE) to generate target radio propagation channels. For the fourth-generation (4G) and previous generation communication technologies, the bandwidth is usually narrow, e.g. up to 20 MHz for singular-carrier LTE signals. Some of the current commercially available channel emulators can support emulating channels with a bandwidth up to 160 MHz [5], which sufficiently cover the need for those signals. However, with the development of the fifth-generation (5G), a much wider bandwidth, such as 400 MHz for frequency range 2 (FR2) [6], is expected to be utilized. Therefore, methods to extend the current channel emulator bandwidth are needed to meet the coming wideband signals.

One of the methods, so called band stitching, is to combine multiple logic channels in the channel emulator into one to form a wider bandwidth [7]. This method makes use of mostly the existing resources in the channel emulator, so it is a straight-up approach compared to designing new hardware.

In this paper, we go through the principle of band stitching for channel emulators, and put a focus on the calibration process of this method. Simulation analysis is done to investigate the effect of calibration on the final performance of the formed wider logic channel.

II. Methods

A. Schematics

The schematics for stitching two logic channels for a single-input single-output (SISO) and a 2×2 MIMO system are shown in Fig. 1. The schematic for the SISO system is detailed in the following, and that for the MIMO system can be viewed as a simple step-up from the SISO case.

In Fig. 1(a), a radio frequency (RF) signal $x_{RF}(t, f)$ is first down-converted by mixing with a local oscillator frequency f_{LO}. Here, t and f denote the time and frequency, respectively. The resulting intermediate frequency (IF) signal $x_{IF}(t, f)$ is split to two identical signals via a splitter (Σ). The IF signal $x_{IF}(t, f)$ is further mixed with different subband IF frequencies $f_{IF_{sub_n}}$ in each branch. The resulting baseband signal $x_{b_n}(t, f)$, with $n = 1, ..., N$ being the index of subbands, is sampled by the analog-to-digital converter (A/D). The target channel in baseband $h_{b_n}(t, f)$ is realized via generating several delay taps (TDL) in the digital domain. The amplitude and phase of each tap is assigned according to the target channel. In addition, the filter shaping the frequency response of the channel is also implemented digitally in this block, i.e. in the finite impulse response (FIR) channel. This block can be realized via e.g. field programmable gate arrays (FPGA) [8]. After multiplying the input signal $x_{b_n}(t, f)$ with $h_{b_n}(t, f)$, a up-converting process is followed similar to the down-converting phase, and the final faded signal $y_{RF}(t, f)$ is obtained. Note that there is a configurable attenuator and phase shifter in each branch so that the power and phase of each branch can be tuned.

This schematic can be easily extended for a 2×2 MIMO system as shown in Fig. 1(b). The target channel matrix

$$\boldsymbol{H} = \begin{bmatrix} h_{11} & h_{12} \\ h_{21} & h_{22} \end{bmatrix}, \tag{1}$$

is emulated by stitching two logic channels for each entry to extend the bandwidth. The time and frequency dependency is omitted in (1) for brevity. A larger bandwidth can be realized by combining more logic channels, and a higher order MIMO channel can be emulated in the same principle similarly.

B. Signal models

For brevity and without loss of generality, we focus on the SISO case in Fig. 1(a) hereafter. Given a radio propagation channel consisting of L taps, the channel coefficients for the nth subband branch can be written as

$$h_{b_n}(t, f) = \sum_{l=1}^{L} \alpha_l(t) \cdot e^{-j2\pi f_{IF_{sub_n}} \tau_l(t)} \cdot s(f - f_{IF_{sub_n}}), \tag{2}$$

where $\alpha_l(t)$ and $\tau_l(t)$ are the complex amplitude and delay of the lth tap at time t, respectively. The term $s(f - f_{IF_{sub_n}})$ is the filter response for the nth subband.

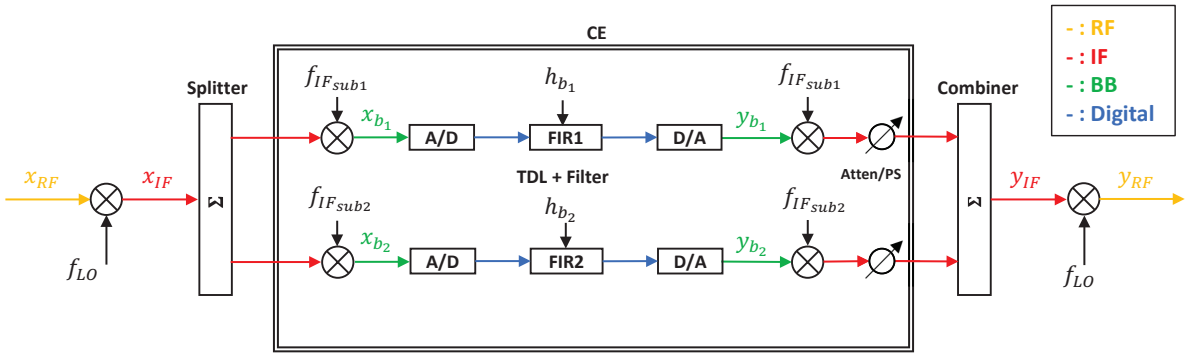

(a)

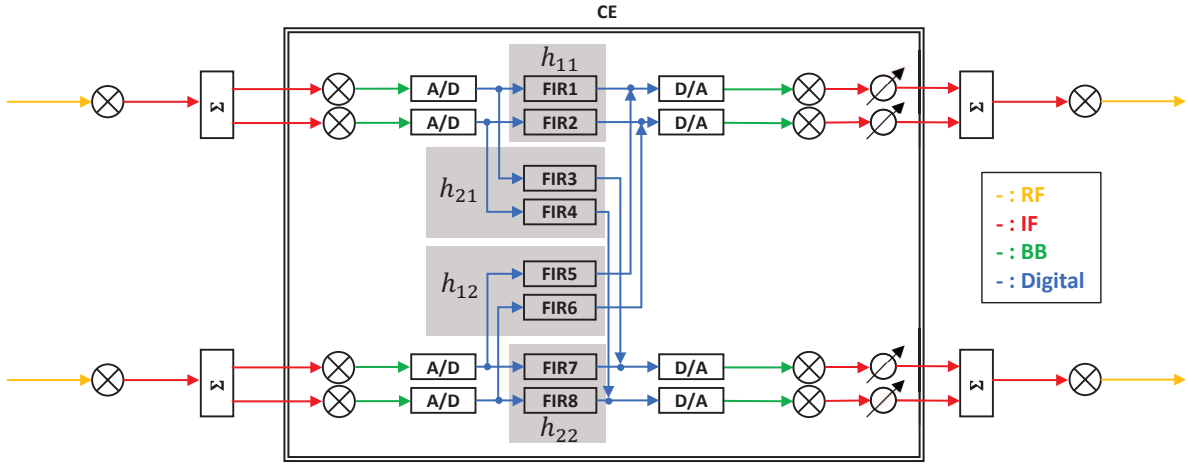

(b)

Fig. 1. Schematics for stitching two logic channels for (a) a single-input single-output (SISO) system and (b) a 2×2 MIMO system. Note that the time and frequency dependency of the signals is omitted for brevity.

The raised cosine filter is considered in this work, while other proper filters can also be used in general. The delay τ domain representation of the raised cosine filter $s(f)$ can be expressed as

$$s(\tau) = sinc(\tau/T) \cdot \frac{cos(\pi\beta\tau/T)}{1 - 4\beta^2\tau^2/T^2}, \tag{3}$$

where T is the reciprocal of the bandwidth of each logic channel B_s, and in our case B_s is the same as the frequency interval between consecutive subband IF frequencies $f_{IF_{sub_n}}$. The term $\beta \in [0, 1]$ is the roll-off factor, and it is determined by

$$\beta = \frac{B_{stop}}{B_s} - 1, \tag{4}$$

where B_{stop} is the stop bandwidth of the filter. The frequency response of the filter $s(f)$ can be obtained by Fourier transform over $s(\tau)$.

The total response of the combined channel reads

$$h_b(t, f) = \sum_{n=1}^{N} h_{b_n}(t, f), \tag{5}$$

and the contribution of the lth tap taking (2) and (5) into account, i.e.

$$h_b^l(t, f) = \sum_{n=1}^{N} \alpha_l(t) \cdot e^{-j2\pi f_{IF_{sub_n}} \tau_l(t)} \cdot s(f - f_{IF_{sub_n}}), \tag{6}$$

are expected to comply with or at least approximate that of a single tap channel, i.e. the magnitude of $h_b^l(t, f)$ being the same in the bands of interest and the slope of the phase response of $h_b^l(t, f)$ corresponding to the tap delay $\tau_l(t)$, after some tuning in β.

C. Calibration

A vector network analyzer (VNA) or similar kinds can be used to measure the frequency response of each branch sequentially while turning off the other branches.

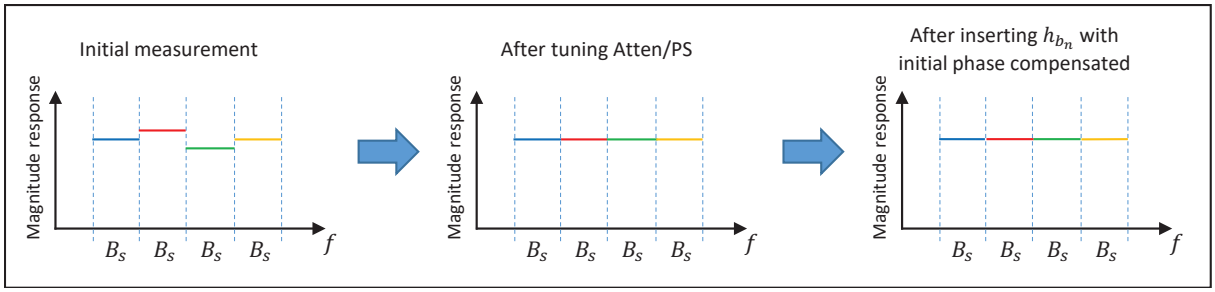

(a)

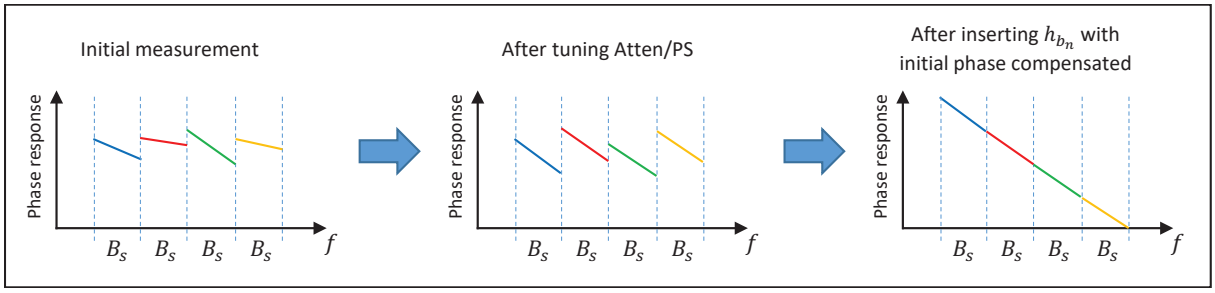

(b)

Fig. 2. Diagrams showing the effect of the calibration in different steps on the frequency response in (a) magnitude and (b) phase. An example of the 4-band stitching with ideal filters is shown here for illustration. Different colors indicate different subbands.

In the calibration phase, the FIR channel, if possible, can be set to a "bypass" mode where only a single tap with zero time delay and unity amplitude is realized. When this option is not available, one can also set the FIR channel to a single tap with a small amount of delay, and subtract that amount from the TDL model during testing. In fact, even when a zero delay is set in the FIR channel, it still takes some time for the signals to propagate in the branch between components. In this case, the propagation delay can be estimated from the VNA measurement, and tuning the configurable attenuator and phase shifter can align the delay and gain in different branches. In addition, the initial phase of each branch at $f_{IF_{sub_n}}$ can be read from the measurement. Finally, the baseband channel coefficients $h_{b_n}(t, f)$ for each subband shall be calculated according to (2), and inserted to the FIR channel as the complex amplitude of that tap with the initial phase compensated.

After the tuning and alignment across branches is done, a flat frequency response in magnitude and continuous phase response after unwrapping with its slope matching the estimated delay is expected to see in the VNA measurement in the total band of interest. With that, a wider bandwidth, i.e. $(N \cdot B_s)$, can be realized via stitching N logic channels. The diagrams showing the effect of the calibration on the frequency response in magnitude and phase after different operations are shown in Fig. 2.

Nevertheless, as far as the authors are concerned, commercial channel emulators are built in high quality. Therefore, the initial misalignment in amplitude and phase as shown in the left most subplots in Fig. 2 might be small and negligible. In this case, a common way of calibrating different branches is to tune the reconfigurable phase shifters exhaustively so that the unwrapped phase is approximately continuous at the transition between adjacent subbands [7]. This method is intuitive but time consuming. Compared to this time consuming method, the method detailed previously is more efficient and explanatory from the signal model stand point.

III. Simulation Results

In the simulation, the raised cosine filter with parameter $B_s = 135$ MHz and $B_{stop} = 170$ MHz is implemented according to (3) and (4). The resulting filter response $s(\tau)$ and $s(f)$ in the delay and frequency domain are shown in Fig. 3, respectively.

Our objective in this work is to form a combined bandwidth of 500 MHz, so 4 logic channels, each of which has 135 MHz bandwidth, are stitched together.

As shown in Fig. 2(b), the slopes of the phase responses of different branches need to be the same, which can be realized by tuning the delay of each branch. Moreover, the phase responses between consecutive branches need to be connected end to end. This is realized by compensating the initial phase of each branch in h_{b_n} as mentioned in Section II-C. If the initial phase of each branch is not compensated, phase jump would occur at the junctions between adjacent subbands. However, the phase jump ranges in $(-180°, 180°)$. Compared to the large scale of the unwrapped phase response over the total band of interest, this jump is probably unnoticeable, and hence overlooked sometimes. Note that the stitching performance might potentially deteriorate due to this. To investigate the effect of the phase jump on the stitching performance, we designed two cases in the simulation, i.e. one with the initial phase compensation and one without the compensation.

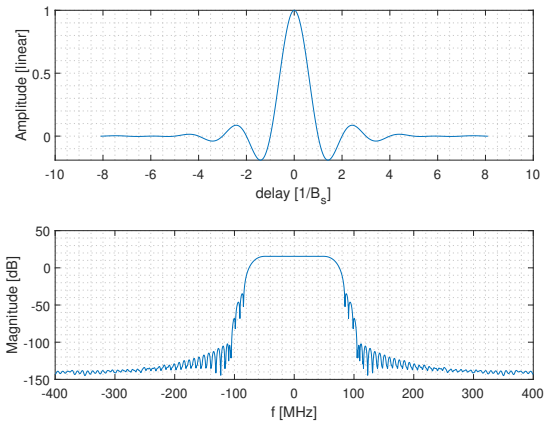

Fig. 3. The filter response in the (top) delay and (bottom) frequency domain. $B_s = 135$ MHz and $B_{stop} = 170$ MHz.

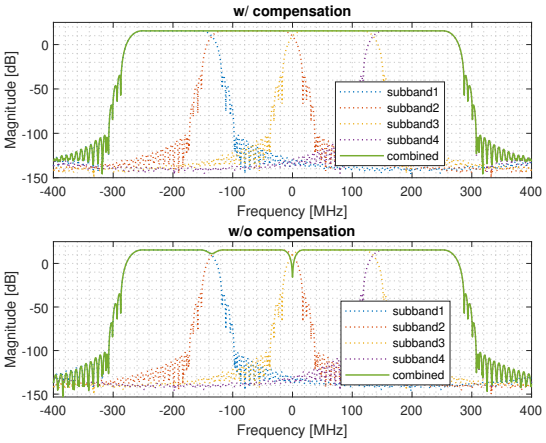

Fig. 5. The frequency response of the 1-tap TDL channel with the combined 500 MHz bandwidth. (Top) the case with the initial phase compensation, and (bottom) the case without the compensation.

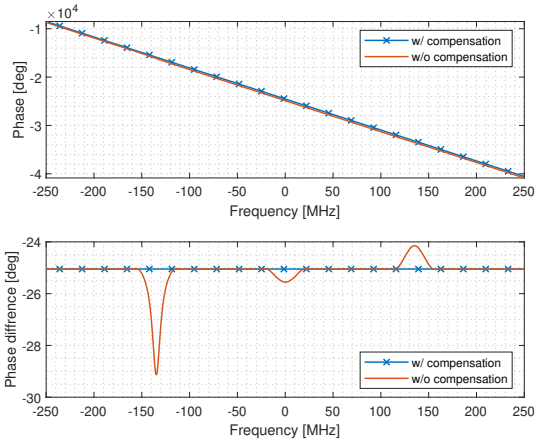

Fig. 4. The phase response of the 1-tap TDL channel with the combined 500 MHz bandwidth. (Top) the unwrapped phase against frequency, and (bottom) its first-order difference.

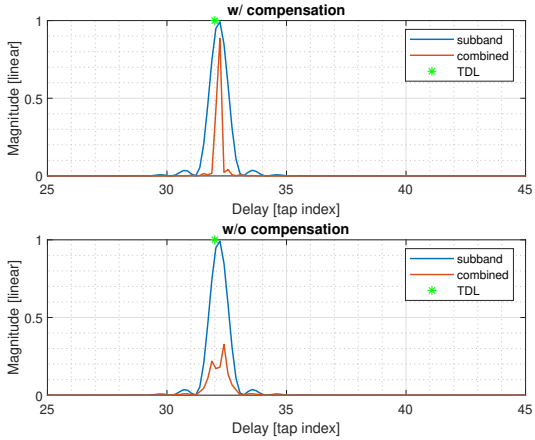

Fig. 6. The power delay profile of the 1-tap TDL channel with the combined 500 MHz bandwidth calculated by the Fourier transform. (Top) the case with the initial phase compensation, and (bottom) the case without the compensation.

The initial phase of each logic channel is generated randomly. A 1-tap TDL channel is generated for the calibration process. The phase responses for the two cases are shown in Fig. 4. As expected, the phase jump is more noticeable in the first-order difference of the phase response for the case without the initial phase compensation.

Fig. 5 shows the magnitude of the frequency response of the combined 500 MHz channel for both cases. We can see deep drops in magnitude at the junctions between adjacent subbands in the case without the initial phase compensation, which justifies the necessity of the compensation despite the insignificance of the phase jump in the big picture over the total band as in Fig. 4(top).

Fig. 6 shows the power delay profile of 1-tap TDL channel calculated from the frequency response by the inverse Fourier transform for both cases. The peak of the combined channel is out of shape in the case without the initial phase compensation compared to that with the compensation. Nonetheless, a higher delay resolution is achieved in the combined channel compared to that in the single subband channel as shown in Fig. 6(top) due to the larger combined bandwidth.

Finally, we show the frequency response and the power delay profile of a 4-tap TDL channel with the combined bandwidth in Fig. 7. The 4-tap TDL channel is well generated with the combined 500 MHz bandwidth, and higher delay resolution is achieved compared to the single subband case.

IV. Conclusion

The principle of band-stitching for channel emulation is revisited. We put a focus on the calibration phase of the process. It is found a wider bandwidth can be realized via combining multiple logic channels into one. The effect of phase jump at the junctions between adjacent subbands on the stitching performance is investigated via simulation. The results show though the phase jump is small compared to the

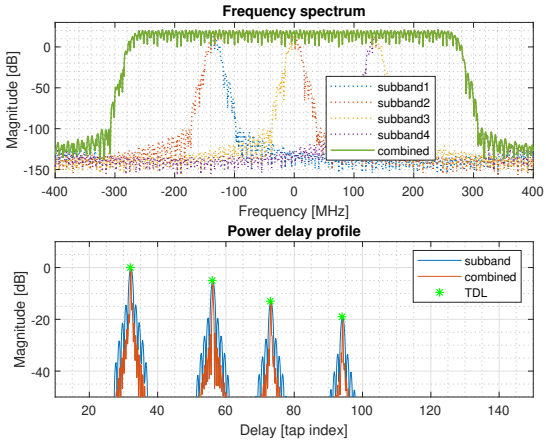

Fig. 7. (Top) the frequency response and (bottom) the power delay profile of the 4-tap TDL channel with the combined 500 MHz bandwidth.

total phase change over the band of interest, it can lead to deep drops in the frequency response and out-of-shape peaks in the power delay profile for the combined channel. Therefore, it is important to compensate that in the calibration phase.

ACKNOWLEDGMENT

REFERENCES

[1] P. Kyösti, T. Jämsä, and J.-P. Nuutinen, "Channel modelling for multi-probe over-the-air MIMO testing," *International Journal of Antennas and Propagation*, vol. 2012, 2012.

[2] W. Fan, X. Carreño, J. Ø. Nielsen, K. Olesen, M. B. Knudsen, and G. F. Pedersen, "Measurement verification of plane wave synthesis technique based on multi-probe MIMO-OTA setup," in *IEEE Vehicular Technology Conference (VTC Fall)*, 2012, pp. 1–5.

[3] W. Yu, Y. Qi, S. Member, K. Liu, Y. Xu, and A. Two-stage, "Radiated Two-Stage Method for LTE MIMO User," *IEEE Transactions on Electromagnetic Compatibility*, vol. 56, no. 6, pp. 1691–1696, 2014.

[4] 3GPP, "Verification of radiated multi-antenna reception performance of User Equipment (UE)," Technical Specification Group Radio Access Network, Tech. Rep. 3GPP TR 37.977 V14.3.0, 2017.

[5] Keysight, "Keysight Technologies Propsim F8 Channel Emulator," Tech. Rep. [Online]. Available: https://literature.cdn.keysight.com/litweb/pdf/5992-1609EN.pdf?id=2754121

[6] 3GPP, "5G; NR; Base Station (BS) radio transmission and reception," Tech. Rep. 3GPP TS 38.104 version 15.2.0 Release 15, 2019. [Online]. Available: https://portal.etsi.org/TB/ETSIDeliverableStatus.aspx

[7] W. Fan, P. Kyosti, L. Hentila, and G. F. Pedersen, "A flexible millimeter-wave radio channel emulator design with experimental validations," *IEEE Transactions on Antennas and Propagation*, vol. 66, no. 11, pp. 6446–6451, 2018.

[8] K. C. Borries, G. Judd, D. D. Stancil, and P. Steenkiste, "FPGA-based channel simulator for a wireless network emulator," *IEEE Vehicular Technology Conference*, no. April 2009, 2009.